COMPUTATION OF RIEMANN SOLUTIONS USING THE DAFERMOS REGULARIZATION AND CONTINUATION

STEPHEN SCHECTER, BRADLEY J. PLOHR, AND DAN MARCHESIN

Abstract. We present a numerical method, based on the Dafermos regularization, for computing a one-parameter family of Riemann solutions of a system of conservation laws. This family corresponds to varying either the left or right state of the Riemann problem. The Riemann solutions are required to have shock waves that satisfy the viscous profile criterion prescribed by the physical model. The method uses standard continuation software to solve a boundary-value problem in which the left and right states of the Riemann problem appear as parameters. Because the continuation method can proceed around limit point bifurcations, it can sucessfully compute multiple solutions of a particular Riemann problem, including ones that correspond to unstable solutions of the viscous conservation laws.

1. Introduction

1.1. Conservation laws.

A *system of conservation laws*

$$u_t + f(u)_x = 0, \tag{1.1}$$

where $u(x,t) \in \mathbb{R}^n$ and $f : \mathbb{R}^n \to \mathbb{R}^n$, admits solutions with jump discontinuities called *shock waves*. The simplest take the form

$$u(x,t) = \begin{cases} u_- & \text{for } x < st, \\ u_+ & \text{for } x > st. \end{cases} \tag{1.2}$$

For the shock wave (1.2) to be a weak solution of system (1.1), the triple (u_-, s, u_+) must satisfy the *Rankine-Hugoniot condition*

$$f(u_+) - f(u_-) - s(u_+ - u_-) = 0. \tag{1.3}$$

However, too many discontinuities of the form (1.2) satisfy condition (1.3). The meaningful discontinuities must be selected based on physical modeling.

A *viscous regularization* of system (1.1) is a partial differential equation of the form

$$u_t + f(u)_x = \epsilon(B(u)u_x)_x, \tag{1.4}$$

where $\epsilon > 0$ and $B(u)$ is an $n \times n$ matrix for which all eigenvalues have positive real part. A system of conservation laws (1.1) as an approximation of a viscous system (1.4) obtained by setting $\epsilon = 0$ in a situation where ϵ is small. Courant and Friedrichs [4] and Gelfand [8]

Date: September, 2002.

1991 *Mathematics Subject Classification.* 35L65, 35L67, 35K50.

Key words and phrases. conservation law, viscous conservation law, Riemann problem, viscous profile, Dafermos regularization, continuation, numerical method.

This work was supported in part by: the NSF under Grant DMS-9973105; the NSF under Grant DMS-9732876; the DOE under Grant DE-FG02-90ER25084; the ARO under Grant 38338-MA; CNPq under Grant 300204/83-3; and ANP under Grant PRH-32.

therefore proposed that, if system (1.1) arises in this way, then a shock wave (1.2) should be admitted as a solution of system (1.1) provided that Eq. (1.4) has a traveling wave solution

$$u^\epsilon(x,t) = \hat{u}\left(\frac{x - st}{\epsilon}\right) \tag{1.5}$$

that satisfies the boundary conditions

$$\hat{u}(-\infty) = u_-, \quad \hat{u}(+\infty) = u_+. \tag{1.6}$$

Such a solution u^ϵ converges to the shock wave (1.2) as $\epsilon \to 0^+$. If a traveling wave solution of Eq. (1.4) exists, then the shock wave (1.2) is said to satisfy the *viscous profile criterion* for $B(u)$. A traveling wave solution of Eq. (1.4) satisfying the boundary conditions (1.6) exists if and only if the *traveling wave ODE*

$$\dot{u} = B(u)^{-1}\left[f(u) - f(u_-) - s(u - u_-)\right] \tag{1.7}$$

has an equilibrium at u_+ (it automatically has one at u_-) and a connecting orbit from u_- to u_+.

Suppose that $Df(u_-)$ is *strictly hyperbolic* (*i.e.*, its the eigenvalues real and distinct) and the genuine nonlinearity condition [21] is satisfied at u_-. Then for each eigenvalue λ of $Df(u_-)$, there exists a curve $u_+(s)$, defined for s near λ, with $u_+(\lambda) = u_-$, and tangent at u_- to the corresponding eigendirection of $Df(u_-)$, such that each triple $(u_-, s, u_+(s))$ satisfies the Rankine-Hugoniot condition (1.3) (see, *e.g.*, Ref. [21]). If, in addition, $B(u_-)$ is *strictly stable* with respect to $Df(u_-)$, then for s sufficiently close to λ, there is a connecting orbit of the traveling wave ODE (1.7) joining u_- to $u_+(s)$ if and only if $s < \lambda$ [16]. Thus, for u_+ close to u_-, existence of the connecting orbit is rather insensitive to the viscosity matrix that is used. However, for a solution (u_-, s, u_+) of the Rankine-Hugoniot condition (1.3) with u_+ farther from u_-, existence of a connecting orbit depends strongly on $B(u)$.

1.2. **Riemann problems.** The most basic initial-value problem for the system of conservation laws (1.1) is the *Riemann problem*:

$$u(x,0) = \begin{cases} u_L & \text{for } x < 0, \\ u_R & \text{for } x > 0. \end{cases} \tag{1.8}$$

In conformance with the scale-invariance of system (1.1) and the initial conditions (1.8), a solution is expected to have the form $u(x,t) = \hat{u}(\xi)$, where $\xi = x/t$, consisting of constant parts, continuously changing parts (*rarefaction waves*), and jump discontinuities (shock waves). Shock waves occur when

$$\lim_{\xi \to s-} \hat{u}(\xi) = u_- \neq u_+ = \lim_{\xi \to s+} \hat{u}(\xi). \tag{1.9}$$

One requires each such triple (u_-, s, u_+) to satisfy the viscous profile criterion for $B(u)$.

It is known that, even when shock waves are required to satisfy the viscous profile criterion, certain Riemann problems can have multiple solutions. At first sight, this fact is disconcerting, because the Riemann problem is formally an initial-value problem. In fact, the Riemann initial data for the invicid conservation laws should be regarded as an idealization of smooth initial data for the viscous conservation laws. In this light, there are two competing length scales in the initial-value problem—the viscous length scale and length scale of smoothing of initial data—and the limiting solution obtained as these length scales vanish can depend on the manner in which the limit is taken.

However, solutions of Riemann problems can also be regarded as asymptotic solutions of system (1.4), and the occurrence of multiple asymptotic solutions is not surprising. More precisely, let u be a solution of the initial/boundary-value problem for system (1.4) with initial and boundary conditions

$$u(x,0) = u_0(x), \tag{1.10}$$

$$\lim_{x\to-\infty} u(x,t) = u_L, \quad \lim_{x\to\infty} u(x,t) = u_R, \tag{1.11}$$

where the initial data u_0 is required to satisfy

$$\lim_{x\to-\infty} u_0(x) = u_L, \quad \lim_{x\to\infty} u_0(x) = u_R. \tag{1.12}$$

Define $\tilde{u}(\xi,t) = u(\xi t, t)$. Then it is believed that, for each fixed ξ, $\tilde{u}(\xi,t)$ typically approaches a limit $\hat{u}(\xi)$ as $t \to \infty$, where $\hat{u}$ solves the Riemann problem (1.1), (1.8) with shock waves that satisfy the viscous profile criterion for $B(u)$. This has been proved in some cases (see, *e.g.*, Refs. [18, 12, 9, 14, 15, 23, 13, 25]) and is seen to occur in numerical simulations.

From this perspective, multiple solutions of a Riemann problem represent multiple asymptotic solutions of the initial/boundary-value problem (1.4), (1.10), (1.11), which are approached for different initial conditions u_0. For an example with three Riemann solutions, Azevedo, Marchesin, Plohr, and Zumbrun [1] have performed analysis and numerical calculations that confirm this picture. Two of the Riemann solutions appear to be stable, in that they attract all nearby solutions; the third appears to be the limit of a codimension-one set of initial conditions, which forms the boundary between the domains of attraction of the first two solutions.

1.3. **Numerical Riemann solvers.** There are many numerical Riemann solvers specialized for particular systems of conservation laws. However, for general systems, there are only a few numerical methods for finding Riemann solutions with shock waves that satisfy a given viscous profile criterion:

(1) Solve the viscous regularization (1.4) for some choice of initial condition satisfying conditions (1.11) and observe the time-asymptotic limit. This method is limited to finding asymptotic solutions that are stable. A variant of this method, which we mention below, is used in Ref. [1].
(2) Piece together wave curves. For $n = 2$, this can be done using the interactive Riemann Problem Package of Isaacson, Marchesin, Plohr *et al.* This method yields, in addition to Riemann solutions, a good understanding of the waves that they comprise, but it is labor-intensive.

In this paper, we propose another numerical method for finding Riemann solutions. This method finds one-parameter families of Riemann solutions, including unstable ones, and is therefore especially useful for studying the bifurcations of Riemann solutions.

Remark. One could solve the inviscid conservation laws (1.1) with Riemann initial data (1.8), but such an approach ignores the viscosity matrix $B(u)$; in problems where the shock waves depend sensitively on the viscosity, the computed solutions are wrong.

An analogy to autonomous ordinary differential equations $\dot{y} = g(y)$, where $y(t) \in \mathbb{R}^m$, is perhaps helpful here. A solution of such an ODE often approaches an equilibrium as $t \to \infty$. Therefore one way to find an equilibrium is to solve an initial-value problem and observe the time-asymptotic limit. A limiting equilibrium is usually asymptotically stable. This method of finding equilibria is analogous to the method (1) above for finding Riemann solutions.

A second numerical approach to finding equilibria of autonomous ODEs applies to one-parameter families $\dot{y} = g(y, \lambda)$, where $y(t) \in \mathbb{R}^m$ and $\lambda \in \mathbb{R}$. The equilibria satisfy $g(y, \lambda) = 0$ and typically form a curve in (y, λ)-space. Suppose that, for some λ_0, an equilibrium y_0 of $\dot{y} = g(y, \lambda_0)$ is known, so that $g(y_0, \lambda_0) = 0$. (The solution (y_0, λ_0) might be available because the equation $g(y, \lambda_0) = 0$ is simple enough to be solved analytically, because it has been solved numerically by Newton's method, or because a stable equilibrium has been found by solving an initial-value problem and observing the time-asymptotic limit.) Then the branch of the curve $g(y, \lambda) = 0$ through (y_0, λ_0) can be computed by a continuation method. Continuation methods work by approximating the tangent vector to the curve, moving a little distance along the tangent vector, and then using Newton's method to return to the curve. They can be designed to accurately compute solutions even at limit points of the curve $g(y, \lambda) = 0$. Thus they can find unstable equilibria.

Continuation methods can also be used to solve ODE boundary-value problems that depend on a parameter. The reason is that a BVP can be regarded as an equation of the form $G(y, \lambda) = 0$, where y lies in a function space. The function space can be approximated by a finite-dimensional one (for example, by discretizing the ODE), and a known solution (y_0, λ_0) can be continued as before.

The numerical method described in this paper is analogous to the continuation method for computing equilibria of a one-parameter family of ODEs. Indeed, an approximate Riemann solution can be regarded as a solution of a boundary-value problem for an ODE, and a standard continuation software package for continuing solutions of BVPs can then used.

1.4. **Dafermos regularization.** The ODE that we solve comes from *Dafermos regularization.* Given a viscous regularization (1.4) of a system of conservation laws (1.1), the associated Dafermos regularization is

$$u_t + f(u)_x = \epsilon t (B(u) u_x)_x \tag{1.13}$$

Like the Riemann problem, but unlike the viscous regularization (1.4), system (1.13) is scale-invariant and therefore has many solutions of the form $u(x, t) = \hat{u}(\xi)$ with $\xi = x/t$. Such a solution satisfies the *Dafermos ODE*

$$[Df(u) - \xi I]\, u' = \epsilon\, [B(u) u']' , \tag{1.14}$$

where the prime denotes differentiation with respect to ξ. Corresponding to the Riemann data (1.8), we impose the boundary conditions

$$u(-\infty) = u_L, \quad u(+\infty) = u_R. \tag{1.15}$$

For the case $B(u) \equiv I$, Dafermos conjectured that solutions of the boundary-value problem (1.14)–(1.15) converge to the corresponding Riemann solution as $\epsilon \to 0^+$. This conjecture has been proved for u_R close to u_L by Tzavaras [24], who takes a sequence of solutions as $\epsilon \to 0^+$, shows that a subsequence converges, and demonstrates that the limit is a Riemann solution.

Recently, Szmolyan [22] studied the boundary-value problem (1.14)–(1.15) for the case $B(u) \equiv I$ using geometric singular perturbation theory. His idea is to regard a Riemann solution as a singular solution ($\epsilon = 0$) and then show that, for small $\epsilon > 0$, there is a nearby solution. Szmolyan proved that for small $\epsilon > 0$, a classical Riemann solution consisting of n

waves, each being a rarefaction or compressive shock wave, has a solution of (1.14)–(1.15) nearby. There is no requirement that u_L and u_R be close.

In our view, a key advantage of the Dafermos regularization is that it applies to general $B(u)$. Schecter [20] makes this point explicit and shows that any structurally stable Riemann solution [19] consisting entirely of shock waves that satisfy the viscous profile criterion for a given $B(u)$ has, for small $\epsilon > 0$, a solution of Eqs. (1.14)–(1.15) nearby. Transitional, or undercompressive, shock waves, which are sensitively dependent on $B(u)$, are explicitly allowed. It is likely that, by analyzing rarefaction and composite waves, one can prove that any structurally stable Riemann solution whose shock waves satisfy the viscous profile criterion has solutions of the corresponding Dafermos regularization nearby.

1.5. **Continuation method.** The preceding discussion motivates trying to approximate Riemann solutions by numerically solving Eqs. (1.14)–(1.15) for small $\epsilon > 0$. We have implemented this idea using AUTO [6], which has been successfully used for many years to conduct continuation and bifurcation studies of ODEs.

We first convert the second-order ODE (1.14) to a first-order ODE by defining $v = \epsilon B(u)u'$:

$$\epsilon u' = B(u)^{-1}v, \tag{1.16}$$

$$\epsilon v' = [Df(u) - \xi I]\, B(u)^{-1}v. \tag{1.17}$$

To use AUTO, we make the ξ-interval finite, namely $-T \le \xi \le T$, and adopt the boundary conditions

$$u(-T) = u_L, \quad u(T) = u_R. \tag{1.18}$$

The interval $-T \le \xi \le T$ must be large enough so that the true solutions for $\xi \in \mathbb{R}$ are close enough to being constant for $|\xi| \ge T$. Since AUTO requires that boundary-value problems be defined on the interval $[0, 1]$, we let $\zeta = (\xi + T)/(2T)$. Then the system (1.16)–(1.17) becomes

$$\frac{du}{d\zeta} = \frac{2T}{\epsilon} B(u)^{-1}v, \tag{1.19}$$

$$\frac{dv}{d\zeta} = \frac{2T}{\epsilon} [Df(u) - \xi I]\, B(u)^{-1}v, \tag{1.20}$$

where $\xi = -T + 2T\zeta$, and the boundary conditions (1.18) become

$$u(0) = u_L, \quad u(1) = u_R. \tag{1.21}$$

We take (ϵ, T, u_L, u_R) to be the vector of parameters, so that AUTO can perform continuation in ϵ, T, or any component of u_L or u_R. We initialize the parameters by choosing ϵ, T, and u_L and setting $u_R = u_L$. One corresponding solution of the boundary-value problem (1.19)–(1.21) is $u(\zeta) \equiv u_L$, $v(\zeta) \equiv 0$. The continuation proceeds from this exact solution.

AUTO discretizes ODE boundary-value problems by the method of orthogonal collocation using piecewise polynomials with 2 to 7 collocation points per mesh interval. The mesh automatically adapts to equidistribute the local discretization error. In the context of the Dafermos ODE, this means that mesh points automatically concentrate near shock waves.

An important feature of AUTO is that continuation proceeds around limit point bifurcations without difficulty. This sometimes allows AUTO to locate multiple solutions of a single Riemann problem, including solutions that are unstable for the corresponding viscous regularization.

2. Computations

In this section we describe some numerical experiments on the system studied in [1]. Let $u = (u_1, u_2)$, $v = (v_1, v_2)$, $u_L = (u_{1L}, u_{2L})$, and $u_R = (u_{1R}, u_{2R})$. As in [1], let

$$f(u) = f(u_1, u_2) = \begin{pmatrix} -\frac{1}{2}u_1^2 + \frac{1}{2}u_2^2 - 0.12u_1 + 0.23u_2 \\ u_1 u_2 - 0.23u_1 - 0.12u_2 \end{pmatrix} \tag{2.1}$$

and

$$B(u) = B(u_1, u_2) = \begin{pmatrix} 1 & 0.7 \\ 0.7 & 1 \end{pmatrix}^{-1}. \tag{2.2}$$

We are interested in Riemann solutions of (1.1) for which the shock waves satisfy the viscous profile criterion for the viscous regularization (1.4). We approximate these Riemann solutions by solving the truncated Dafermos BVP (1.19)–(1.21) with $\epsilon = .0002$ and $T = 1.5$. In all of our numerical experiments, we fix

$$u_L = (u_{1L}, u_{2L}) = (0.366078, 0.308156). \tag{2.3}$$

2.1. **Experiment 1.** We begin by setting u_R equal to u_L, so that the Riemann problem, and our truncated boundary value problem, have a constant solution. Next we use AUTO to continue the solution as u_{2R} is decreased to $u_{2R} = 0.1$. Then we continue the solution by decreasing u_{1R} down to -0.6. Fig. 2.1 shows the resulting bifurcation diagram. A single number is chosen to represent the computed Riemann solution; specifically, we choose the maximum value of v_1 over the solution (recall that $v = \epsilon B(u)u'$). In the bifurcation diagram, this number is plotted *vs.* u_{1R}.

The bifurcation diagram has several interesting features. Evidently, it has two limit points, labeled 5 and 8 (with u_{1R} approximately -0.1 and 0.32, respectively). As a result, for each u_{1R} in the interval defined by the abscissae of points 5 and 8, there are three Riemann solutions. As we discuss in more detail below, this three-fold nonuniqueness of solutions of a Riemann problem is the same as investigated in [1]: a Riemann solution on the lower branch has the classical structure consisting of two waves; one on the middle branch involves three waves, the third wave being a shock wave with a homoclinic connection; and one on the upper branch contains four waves, two being transitional shock waves. Also notice the rather angular bends near point 12 and between points 14 and 15.

Figures 2.2–2.17 show (ζ, u_1)- and (u_1, u_2)-plots of the Riemann solutions corresponding to the points labeled 1 to 17 in the bifurcation diagram. The structure of each labeled Riemann solution is as follows.

1: This solution has a classical structure: a 1-shock is on the left and a 2-shock is on the right. These shocks have a nonzero width because $\epsilon > 0$. (See Fig. 2.2(a).)

2: This solution has the same structure as does 1, but the 1-shock is weaker. (See Fig. 2.2(b).)

3: This solution has a 1-rarefaction on the left and a 2-shock on the right; see Fig. 2.3(a). In the (u_1, u_2)-plane, shown in Fig. 2.3(b), the 1-rarefaction is a short, nearly horizontal, segment leading from u_L to a middle state u_M, and the viscous orbit for the 2-shock leads from u_M to u_R. Also, this plot indicates that the u_R is an attracting spiral, *i.e.*, the corresponding eigenvalues have become complex.

4: The solution has the same structure as does 3, but the eigenvalues at u_R have larger imaginary part. (See Fig. 2.4.)

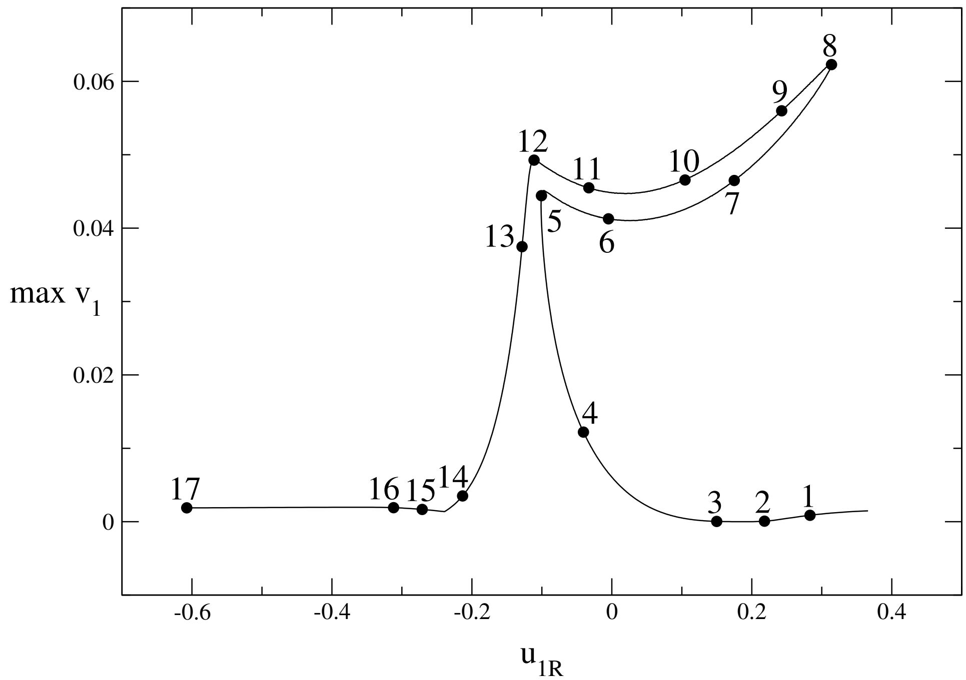

FIGURE 2.1. Bifurcation diagram with $u_{2R} = 0.1$

5: The solution has the same structure as does 4, with a very weak 1-rarefaction. (See Fig. 2.5.) This solution is the limit point 5 in Fig. 2.1. By contrasting with solutions 4 and 6, we see that solution 5 is a point of bifurcation where a 2-shock splits into a homoclinic transitional shock and a 2-shock.

6: This solution contains three waves with distinct speeds: a 1-rarefaction, a homoclinic transitional shock, and a 2-shock. (See Fig. 2.6.) The orbit for the homoclinic shock is the broad loop that (approximately) closes at u_M.

7: The solution has the same structure as does 6, but the eigenvalues at u_R are real and the 1-rarefaction is very weak. (See Fig. 2.7.)

8: The solution has the same structure as does 7, except that the first wave is a 1-shock. (See Fig. 2.8.) This solution is the limit point 8 in Fig. 2.1. By comparing solutions 7 and 9, we see that solution 8 is a point of bifurcation where the homoclinic transitional shock splits into two heteroclinic transitional shocks.

9: This solution contains four waves with distinct speeds: a 1-shock, two heteroclinic transitional shocks, and a 2-shock. (See Fig. 2.9.) The orbit of the slower transitional shock is curved and leads from u_M to $u_{M'}$; the orbit of the faster one is straight and leads from $u_{M'}$ to $u_{M''}$.

10: The solution has the same structure as does 9, except that the first wave is a 1-rarefaction. Also, the eigenvalues at u_R have just become complex. (See Fig. 2.10.)

11: The solution has the same structure as does 10, but the eigenvalues at u_R have larger imaginary part. (See Fig. 2.11.)

12: This solution consists of a very weak 1-shock, a transitional shock with a a curved orbit, and a 2-shock wave for which u_R has complex eigenvalues. (See Fig. 2.12.) This 2-shock is the result of the coalescence of two waves in solution 11, namely, the transitional shock with a straight orbit and the 2-shock. The intermediate state $u_{M''}$ has disappeared.

13: Just as solution 12, this solution has three waves with distinct speeds: a 1-shock, a transitional shock, and a 2-shock. (See Fig. 2.13.)

14: This solution again has a three-wave structure, with the eigenvalues at u_R being real. o(See Fig. 2.14.)

15: This solution again has a four-wave structure: the heteroclinic transitional shock in solution 14 has split into two heteroclinic transitional shocks with almost identical speeds. Also, the 2-shock is very weak. (See Fig. 2.15.)

16: The solution has the same structure as does 15, except that the 2-shock has been replaced by a 2-rarefaction. (See Fig. 2.16.)

17: The solution has three waves: the second transitional shock and the 2-rarefaction have coalesced into a composite 2-wave (in this case, a 2-shock adjacent to a 2-rarefaction). (See Fig. 2.17.) The nearly coincident pairs of shock waves in solutions 15 and 16 have clearly distinct speeds.

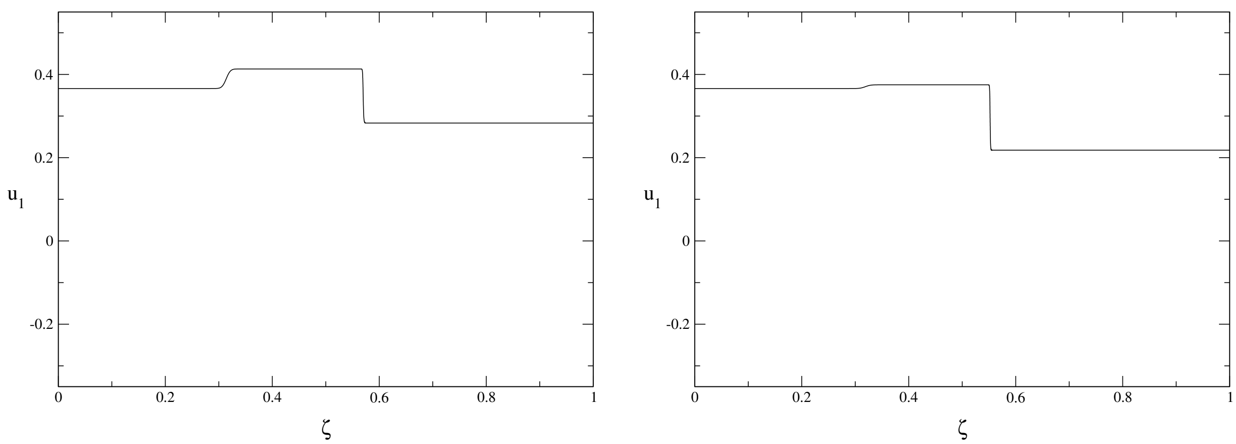

(a) Riemann solution 1 (b) Riemann solution 2

FIGURE 2.2. Riemann solutions 1 and 2: u_1 *vs.* ζ.

Let us make several remarks on these figures.

A. In Riemann solution 2 (see Fig. 2.2(b)), and in several others, shocks are not very sharp. Shocks becomes sharper when ϵ is decreased. For example, starting from Riemann solution 2, we can use AUTO to reduce ϵ from 2×10^{-4} to 10^{-6}. The result is Fig. 2.18, in which the shocks are much sharper.

B. The rather sharp bends in the bifurcation diagram of Fig. 2.1 near points 5, 8, 12 and 15 correspond to the following transitions in the structure of the Riemann solution: (i) splitting of a 2-shock into a homoclinic transitional shock followed by a 2-shock; (ii) splitting of a homoclinic transitional shock into two heteroclinic transitional shocks; (iii) coalescence of a heteroclinic transitional shock and a 2-shock into a 2-shock; (iv) splitting of a heteroclinic transitional shock into two heteroclinic transitional shocks. These transitions can produce corners in the underlying Riemann solution bifurcation diagram [17].

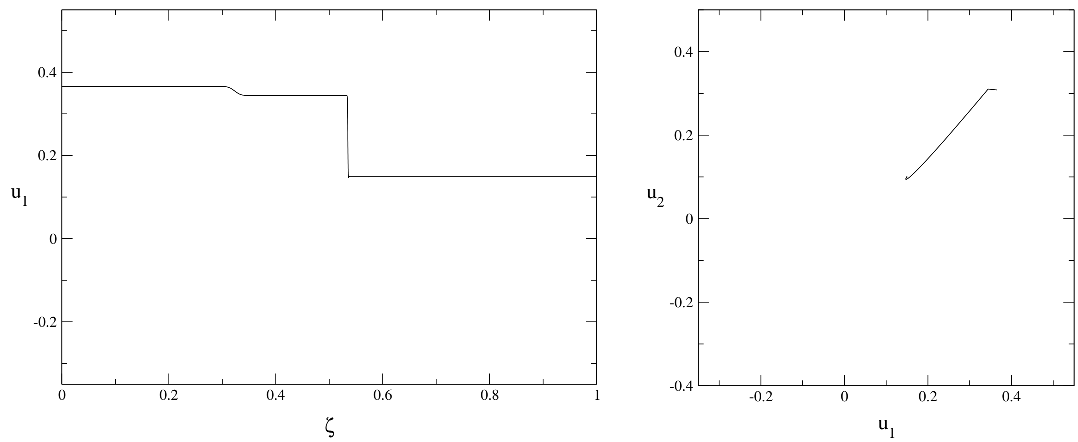

(a) u_1 *vs.* ζ. (b) (u_1, u_2)-plane.

FIGURE 2.3. Riemann solution 3.

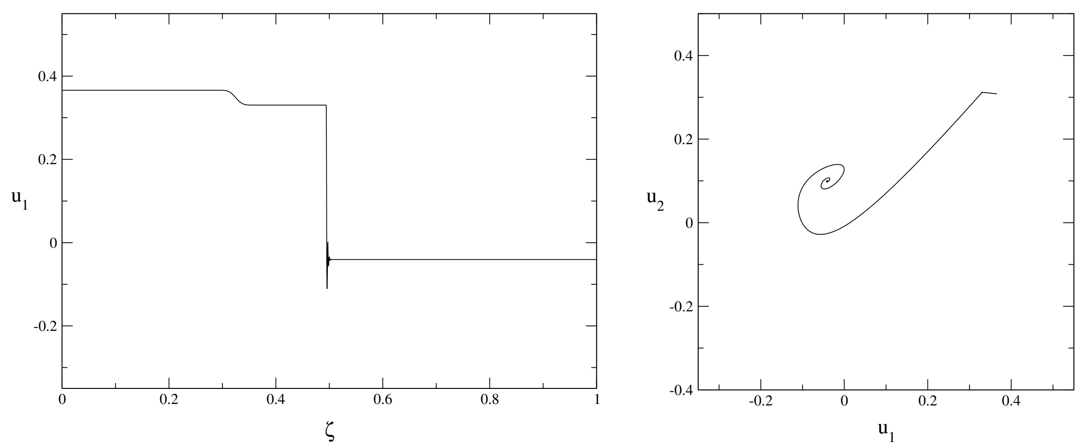

(a) u_1 *vs.* ζ. (b) (u_1, u_2)-plane.

FIGURE 2.4. Riemann solution 4.

C. In the numerical experiments of Ref. [1], Riemann solutions with homoclinic shock waves are unstable. Moreover, in the authors' experience with numerical simulations, shock waves with complex eigenvalues at one end are sometimes unstable. Nonetheless it is useful to consider Riemann solutions that are unstable. For example, in the bifurcation diagram of Fig. 2.1, there are three Riemann solutions for u_{1R} between approximately -0.09 and 0.32. For Riemann solutions 1–3 and 7–9 (u_{1R} between approximately 0.17 and 0.32), the 2-shock has real eigenvalues at both ends, and only solution 7 (on the "middle" solution branch) contains a homoclinic shock. However, our use of a continuation method to find the solutions that are likely to be stable (solutions 1–3, 8, and 9) involved passing through Riemann solutions with complex 2-shocks (solutions 4–6 and 10–13) and homoclinic transitional shocks (solutions 6

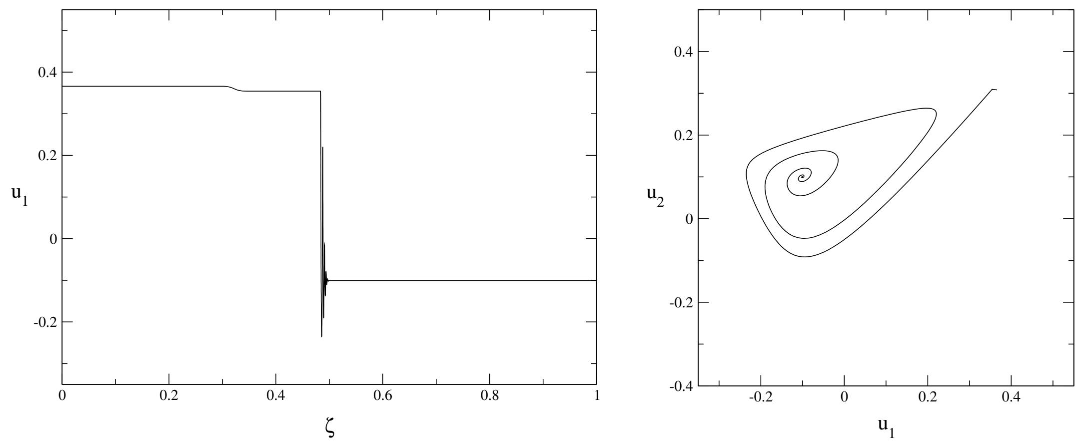

(a) u_1 *vs.* ζ. (b) (u_1, u_2)-plane.

FIGURE 2.5. Riemann solution 5.

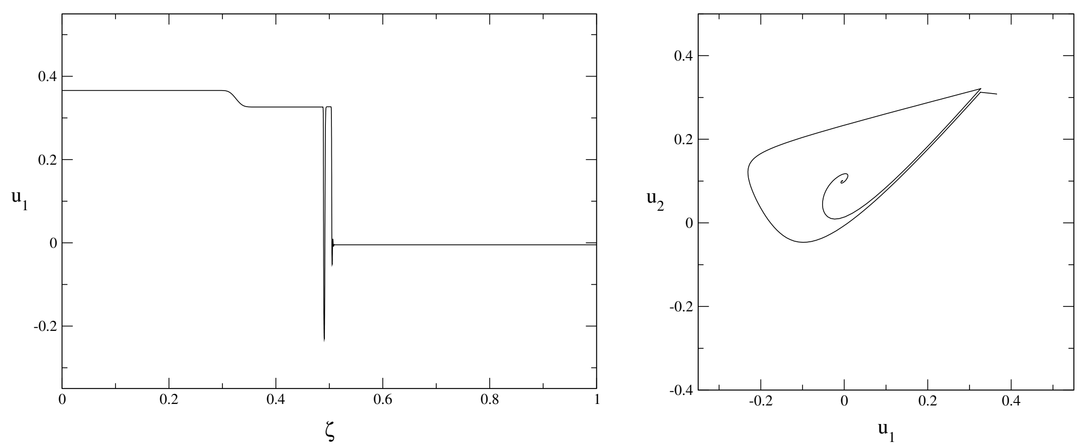

(a) u_1 *vs.* ζ. (b) (u_1, u_2)-plane.

FIGURE 2.6. Riemann solution 6.

and 7). Thus it is useful to allow such possibly unstable solutions to arise during continuation even if one is only interested in stable solutions.

D. One can ask how closely the computed bifurcation diagram of Fig. 2.1 corresponds to the underlying Riemann solution bifurcation diagram near transition points from one structurally stable Riemann solution to another (for example, the two fold points). At present there is no theory about this question.

2.2. **Experiment 2.** Next, starting from $u_R = u_L$, we increase u_{2R} to 0.3998 and then vary u_{1R}. The bifurcation diagram is shown in Fig. 19(a). The point in this bifurcation diagram with $u_{1R} = 0.362832$ is labeled 18; Figs. 20(a) and 20(b) show the (ζ, u_1)- and (u_1, u_2)-plots of this Riemann solution. In fact, no limit points occur during this continuation; the Riemann solution remains classical, throughout, just like solution 18. Note, however, that

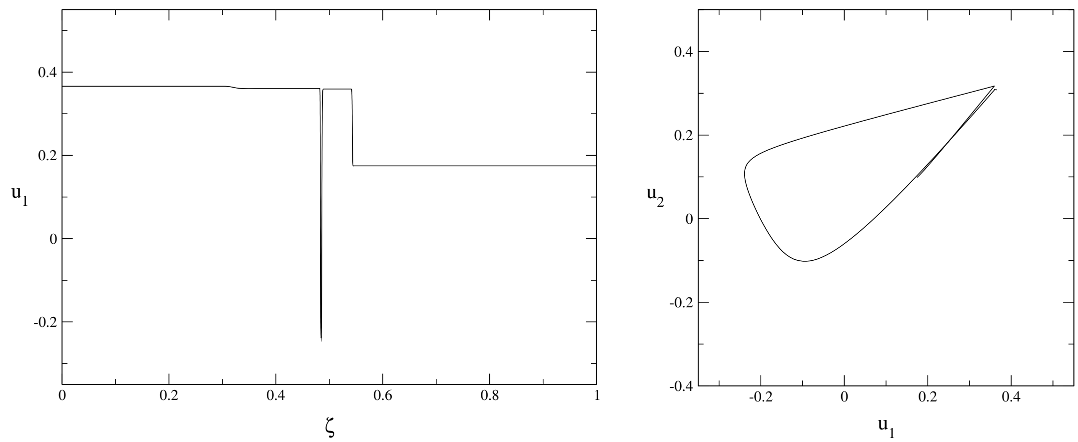

(a) u_1 *vs.* ζ. (b) (u_1, u_2)-plane.

FIGURE 2.7. Riemann solution 7.

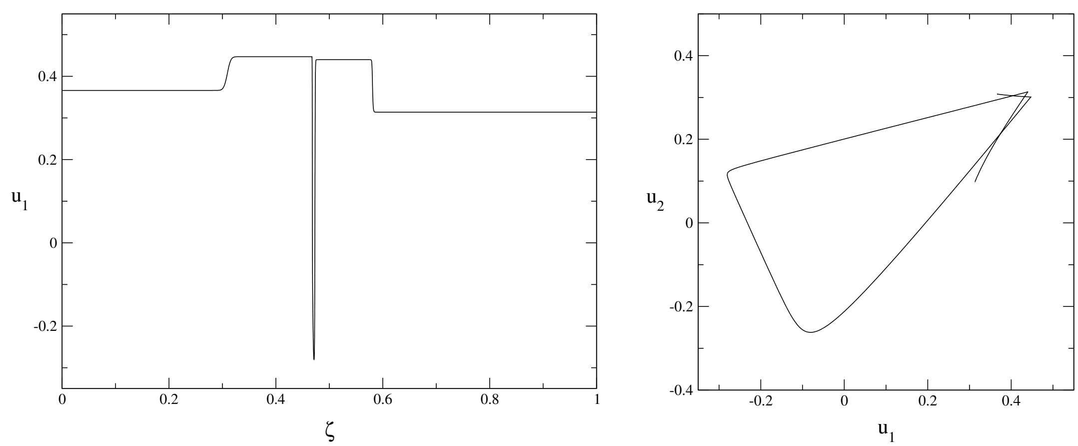

(a) u_1 *vs.* ζ. (b) (u_1, u_2)-plane.

FIGURE 2.8. Riemann solution 8.

in [1], three different Riemann solutions occur for $u_R = (0.362832, 0.3998)$. The additional two solutions, which are labeled 25 and 26 in Fig. 19(b), are found via Experiments 3 and 4.

2.3. **Experiment 3.** To see better how the multiple solutions occur, we start at the limit point 8 in Fig. 2.1 and use AUTO to plot a curve of limit points in the u_R-plane. The resulting curve $\mathcal{L}$ is shown in Fig. 2.21. Note that the line $u_{2R} = 0.1$ meets $\mathcal{L}$ in two points. These points correspond to points 5 and 8 in Fig. 2.1; they are also labeled 5 and 8 here. Also note the occurrence of two cusps. Cusps occur generically along curves of limit points; this is the well-known "cusp catastrophe."

The points of $\mathcal{L}$ correspond approximately to certain Riemann solutions that are not structurally stable, having codimension two at the cusps and otherwise codimension one. The type of codimension-one Riemann solution changes at each cusp:

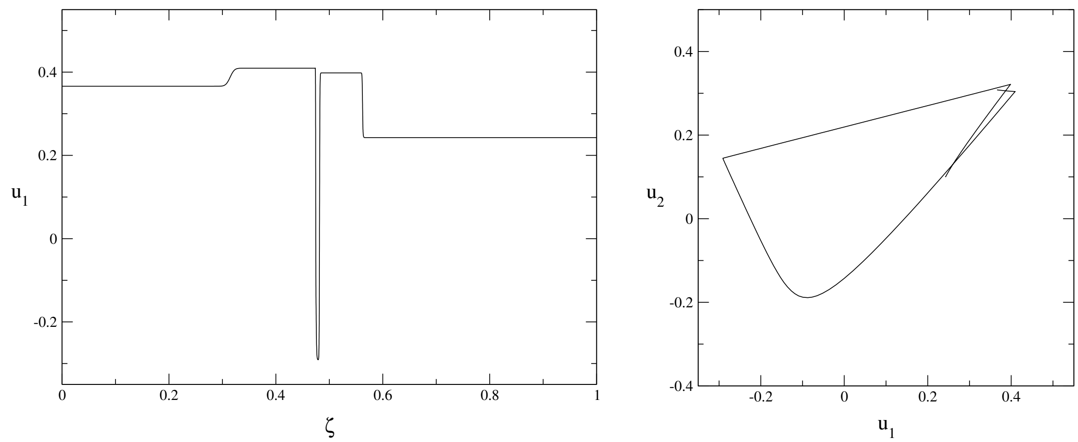

(a) u_1 *vs.* ζ. (b) (u_1, u_2)-plane.

FIGURE 2.9. Riemann solution 9.

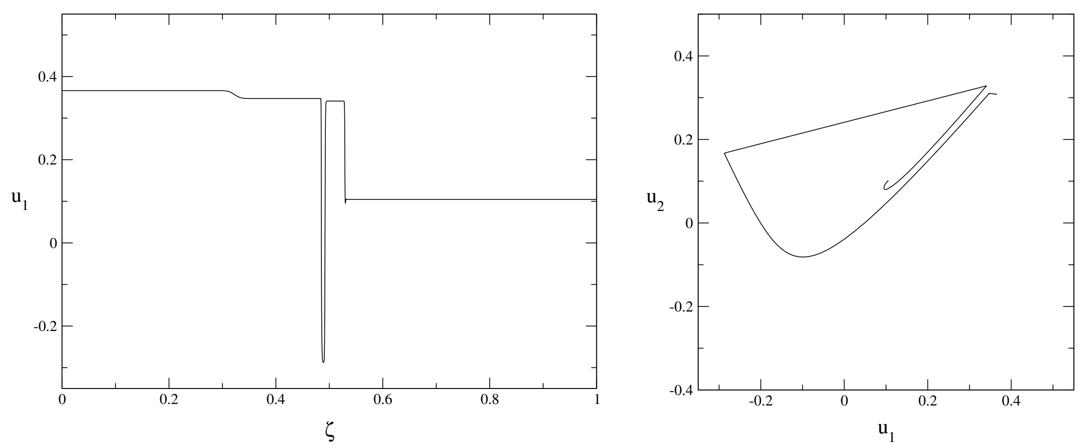

(a) u_1 *vs.* ζ. (b) (u_1, u_2)-plane.

FIGURE 2.10. Riemann solution 10.

A. Points on the upper and lower parts of $\mathcal{L}$ correspond approximately to Riemann solutions consisting of a 1-wave (shock or rarefaction), two heteroclinic transitional shocks (one curved, one straight), and a 2-wave (shock or rarefaction). The two heteroclinic transitional shocks have the same speed; this is what makes the Riemann solution fail to be structurally stable.

Figures 2.22–2.24 show phase portraits for points 19, 20, and 21 on the upper part of $\mathcal{L}$. The corresponding Riemann solutions differ only in that the last wave is a 2-rarefaction for point 19, a 2-shock with real eigenvalues for point 20, and a 2-shock with complex eigenvalues for point 21. All three Riemann solutions (indeed, all Riemann solutions on the top part of $\mathcal{L}$) begin with the same three waves. The top part of $\mathcal{L}$ is, in fact, approximately a portion of the 2-wave curve of the right-most state of the third of these waves.

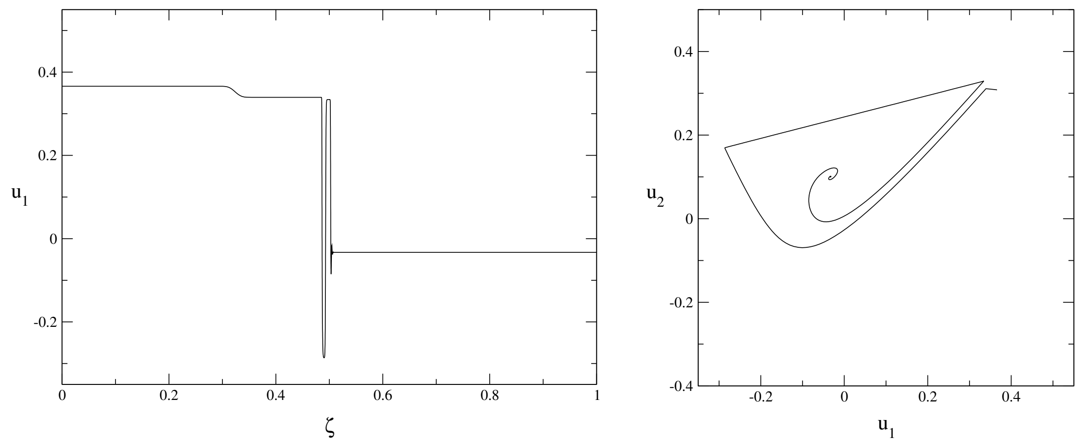

(a) u_1 *vs.* ζ. (b) (u_1, u_2)-plane.

FIGURE 2.11. Riemann solution 11.

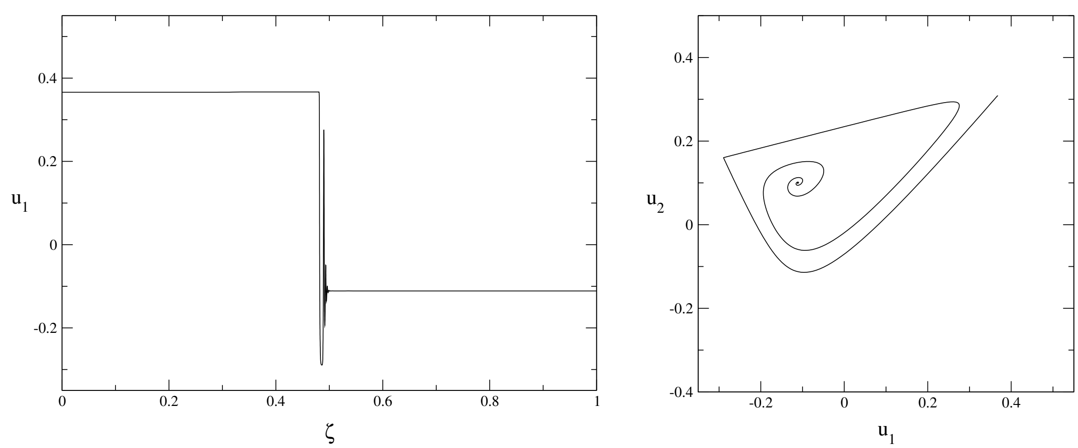

(a) u_1 *vs.* ζ. (b) (u_1, u_2)-plane.

FIGURE 2.12. Riemann solution 12.

Figure 2.25 shows superimposed (ζ, u_1)-plots for these three solutions. At the right in this figure, the highest curve is solution 19, the middle one is solution 20, and the lowest is solution 21. One sees clearly that the three solutions have the same first three waves. One also sees that as one moves to the left along $\mathcal{L}$, the speed of the last wave approaches the common speed of the two heteroclinic shocks. The cusp point is close to a codimension-two Riemann solution in which the two heteroclinic shocks and the 2-shock all have the same speed.

B. Figures 2.26, 2.8, and 2.27 show phase portraits for points 23, 8, and 24 on the lower part of $\mathcal{L}$, and Fig. 2.28 shows superimposed (ζ, u_1)-plots for these solutions. At the right in the last figure, the lowest curve is solution 23, the middle one is solution 8, and the highest is solution 24. These figures are analogous to those for the upper

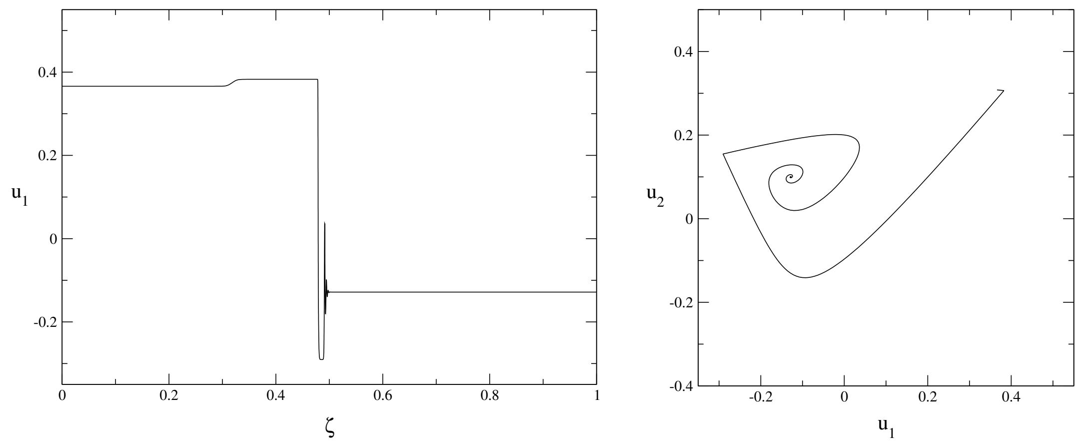

(a) u_1 *vs.* ζ. (b) (u_1, u_2)-plane.

FIGURE 2.13. Riemann solution 13.

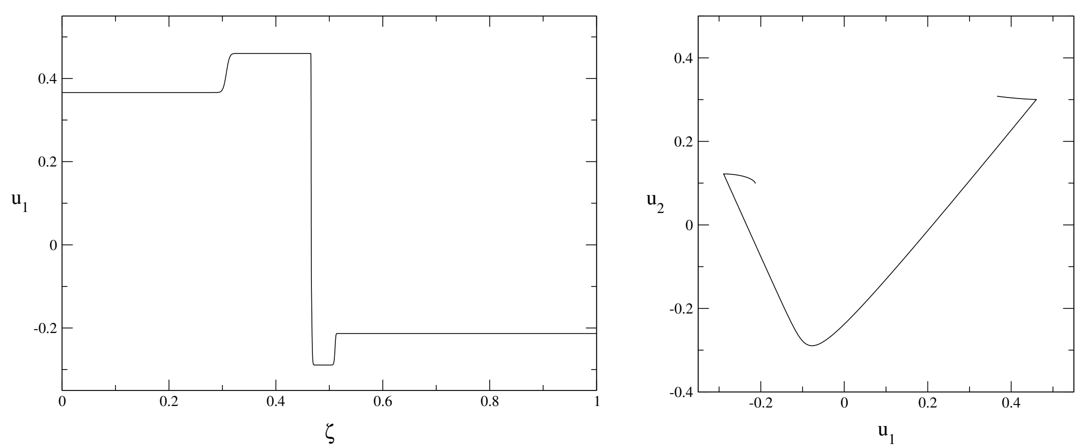

(a) u_1 *vs.* ζ. (b) (u_1, u_2)-plane.

FIGURE 2.14. Riemann solution 14.

part of $\mathcal{L}$. Thus the lower part of $\mathcal{L}$ is also approximately a portion of the 2-wave curve of a certain point.

C. For a point on $\mathcal{L}$ between the cusps, such as point 5 (see Fig. 2.5), the Riemann solution consists of a 1-wave (shock or rarefaction), a homoclinic transitional shock, and a 2-shock, with the homoclinic transitional shock and the 2-shock having the same speed (Because of this coincidence of speeds, the solution has codimension one.) This part of $\mathcal{L}$ is approximately the curve of right states of Riemann solutions of this type with left state U_L.

D. At the both the upper and lower cusp, the homoclinic transitional shock approximately becomes a curved transitional shock followed by a straight transitional shock with the same speed. For example, see Riemann solution 22 in Fig. 2.29.

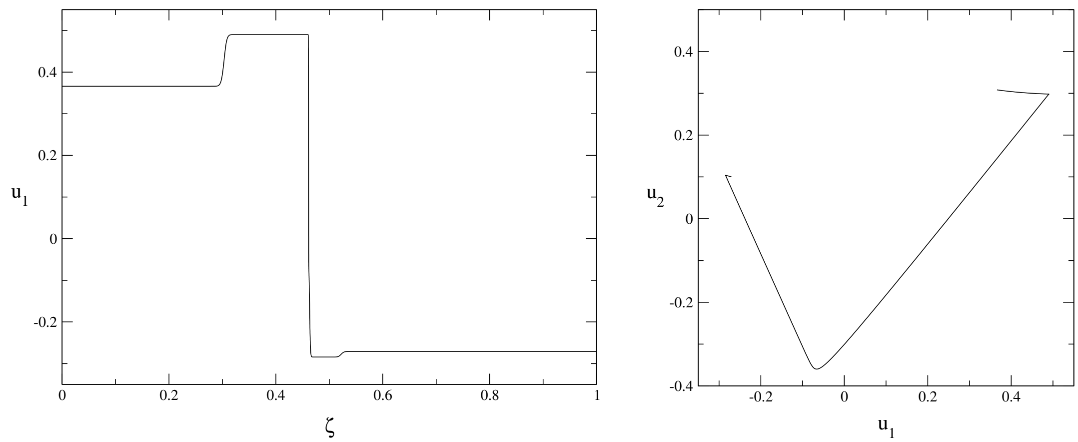

(a) u_1 *vs.* ζ. (b) (u_1, u_2)-plane.

FIGURE 2.15. Riemann solution 15.

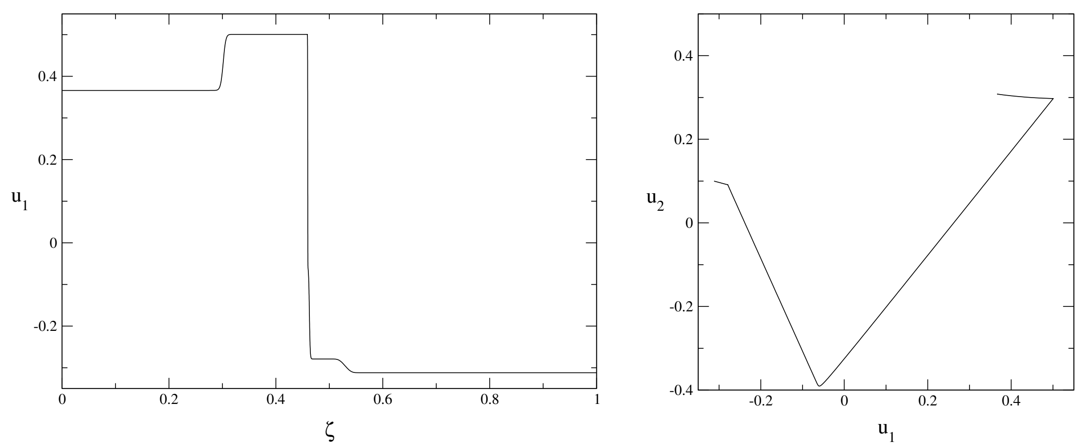

(a) u_1 *vs.* ζ. (b) (u_1, u_2)-plane.

FIGURE 2.16. Riemann solution 16.

Thus $\mathcal{L}$, with the cusps eliminated, comprises three component curves, each being approximately a curve of right states of Riemann solutions with left state U_L and having a certain codimension-one type. If they were exactly curves of Riemann solutions, these component curves would be expected to meet transversally in the space of Riemann solutions [17]. Instead, because they are curves in the space of Dafermos-regularized solutions, they intersect in cusps, as is appropriate for generic fold curves. This difference is illustrated in Fig. 2.30. Thus near the cusps of Fig. 2.1, the solutions computed via Dafermos regularization are quite different from the underlying Riemann solution. At present there is no theory about this issue.

2.4. **Experiment 4.** Finally, we set u_R to correspond to point 19 in Fig. 2.21, which has second component being 0.3998, and vary u_{1R}. The resulting bifurcation diagram is shown

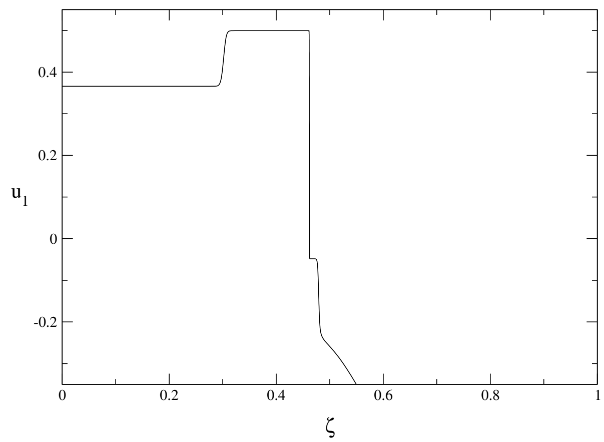

(a) u_1 *vs.* ζ.

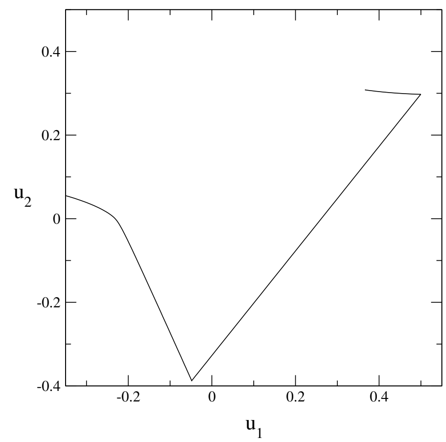

(b) (u_1, u_2)-plane.

FIGURE 2.17. Riemann solution 17.

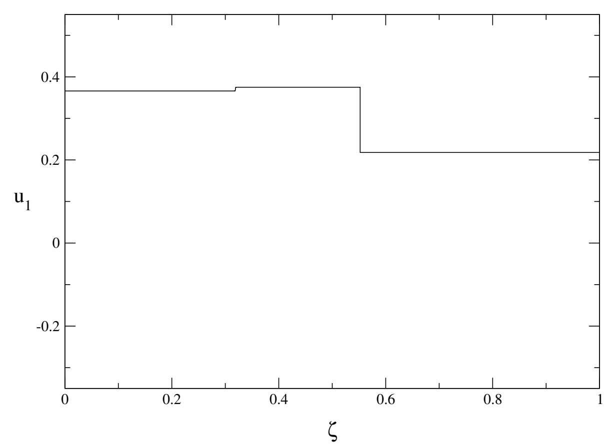

FIGURE 2.18. Riemann solution 2 (calculated with $\epsilon = 10^{-6}$): u_1 *vs.* ζ.

in Fig. 19(b). The points with $u_{1R} = 0.362832$ (which is the u_{1R} component for point 18 in Fig. 19(a)) are labeled 25 and 26.

Figures 2.20, 2.31, and 2.32 show (ζ, u_1)- and (u_1, u_2)-plots of the Riemann solutions corresponding to points 18, 25, and 26. They should be compared to Figs. 2.1–2.3 of [1]. As in Ref. [1], these Riemann solutions can be understood as follows:

18: Classical Riemann solution: 1-rarefaction followed by 2-rarefaction.
25: Three waves with distinct speeds: 1-rarefaction, homoclinic transitional shock, 2-rarefaction.
26: Four waves with distinct speeds: 1-rarefaction, two heteroclinic transitional shocks, 2-rarefaction.

The superposition of Figs. 19(a) and 19(b) is to be contrasted with Fig. 2.1. The superposition corresponds to a slice of Fig. 2.21 with $u_{2R} = 0.3998$, whereas Fig. 2.1 corresponds to a slice with $u_{2R} = 0.1$. Therefore, as u_{2R} is increased from 0.1 to 0.3998, the bifurcation diagram for fixed u_{2R} evolves from Fig. 2.1 to the superposition of Figs. 19(a) and 19(b). A natural expectation is that points 5 and 12 pinch together when the slice approaches the

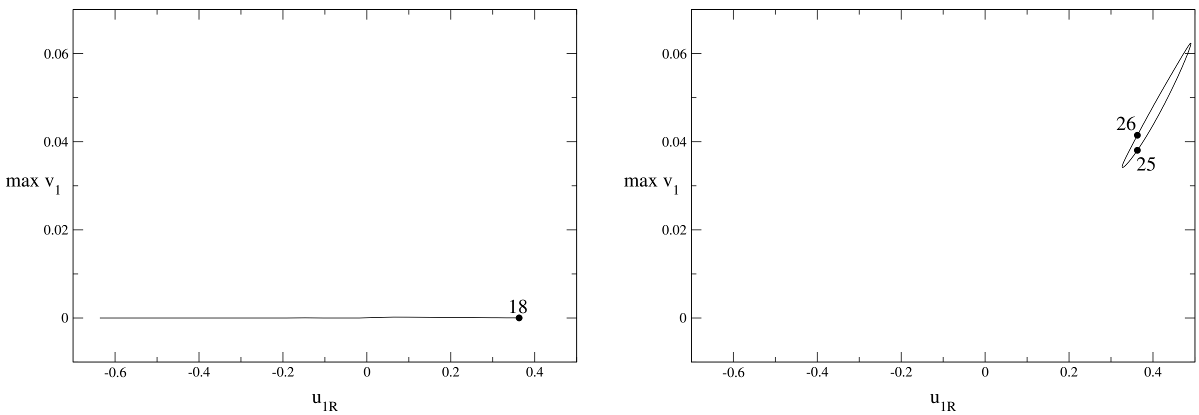

(a) Classical Riemann solutions. (b) Nonclassical Riemann solutions.

FIGURE 2.19. Bifurcation diagram with $u_{2R} = 0.3998$. The two pictures should be superimposed.

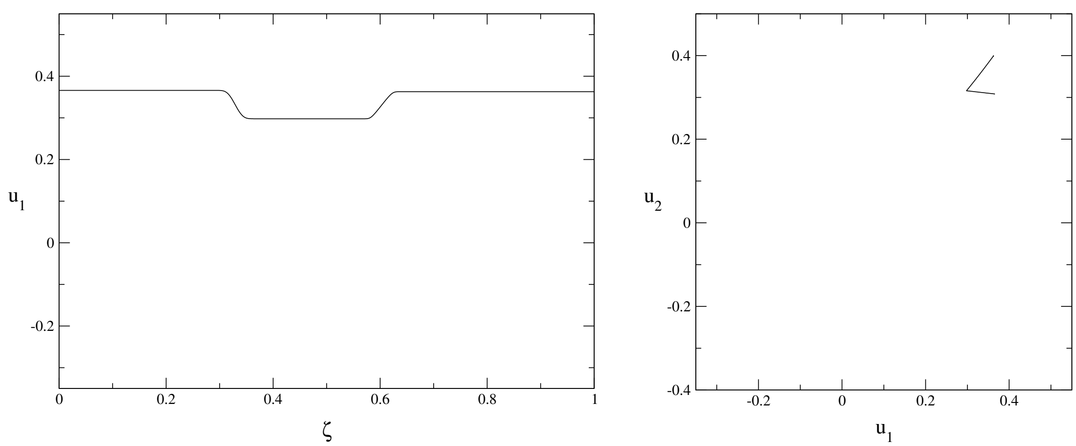

(a) u_1 *vs.* ζ. (b) (u_1, u_2)-plane.

FIGURE 2.20. Riemann solution 18.

upper cusp point of Fig. 2.21 from below, at which stage a bifurcation occurs to two disconnected branches, a branch of "classical" solutions and a loop of "nonclassical" solutions.

3. Conclusion

In this paper we have demonstrated a practical numerical method for constructing Riemann solutions such that all shock waves obey the viscous profile admissibility criterion for a specified viscosity. This method is based continuation of solutions for the Dafermos regularization of the viscous form of the conservation laws. The advantages of this method include its ability to compute solutions containing transitional waves and solutions that are unstable. By devising appropriate paths in the space of Riemann solutions, phenomena such as bifurcation and nonuniqueness can be explored.

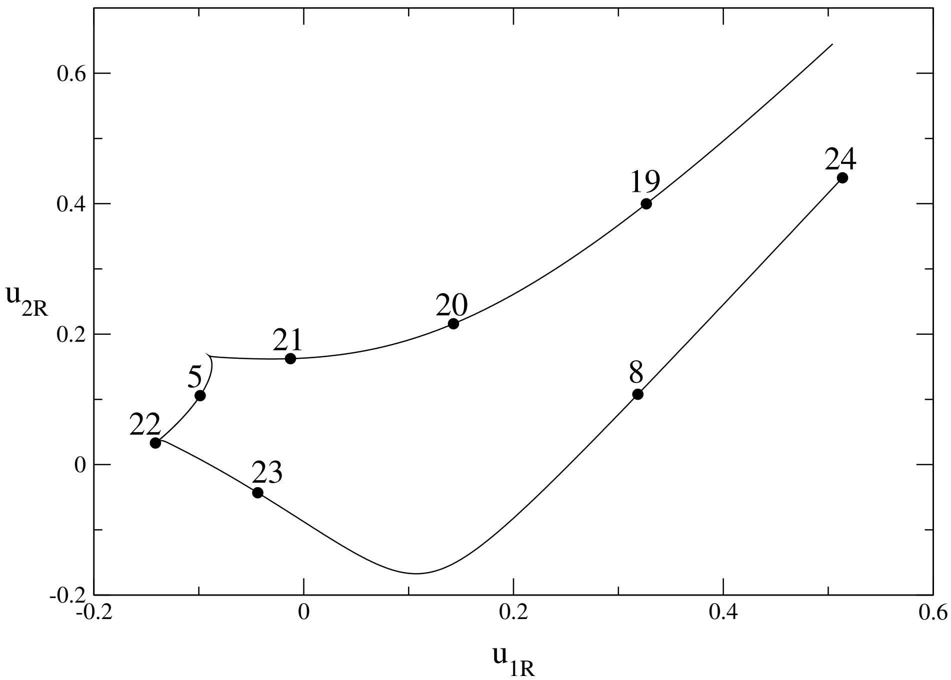

FIGURE 2.21. The curve $\mathcal{L}$ of limit points in the u_R-plane.

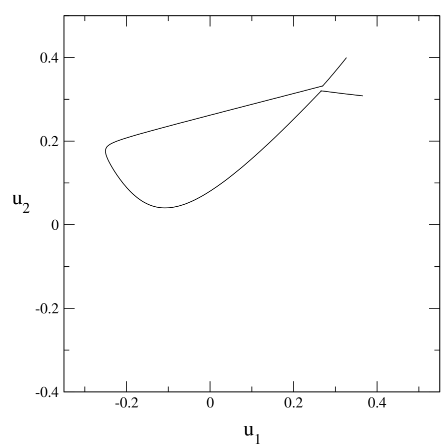

FIGURE 2.22. Riemann solution 19: (u_1, u_2)-plane.

REFERENCES

[1] A. Azevedo, D. Marchesin, B. J. Plohr, and K. Zumbrun, *Nonuniqueness of solutions of Riemann problems*, Zeit. angew. Math. Phys., **47** (1996), 977–998.

[2] A. L. Bertozzi, A. Munch, and M. Shearer, *Undercompressive shocks in thin film flows*, Physica D **134** (1999), 431-464.

[3] S. Čanić, *On the influence of viscosity on Riemann solutions*, J. Dynamics and Differential Equations **9** (1997), 977–998.

[4] R. Courant and K. Friedrichs, "Supersonic flow and shock waves," Interscience, New York, 1948.

[5] C. M. Dafermos, *Solution of the Riemann problem for a class of hyperbolic systems of conservation laws by the viscosity method*, Arch. Rational Mech. Anal. **52** (1973), 1–9.

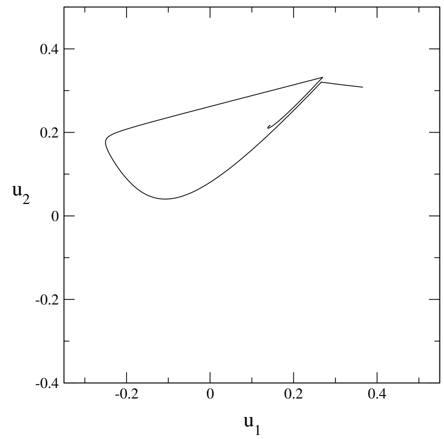

FIGURE 2.23. Riemann solution 20: (u_1, u_2)-plane.

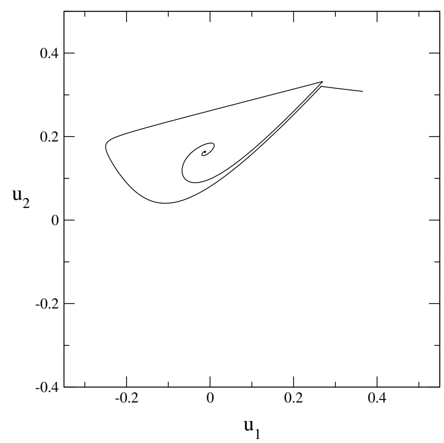

FIGURE 2.24. Riemann solution 21: (u_1, u_2)-plane.

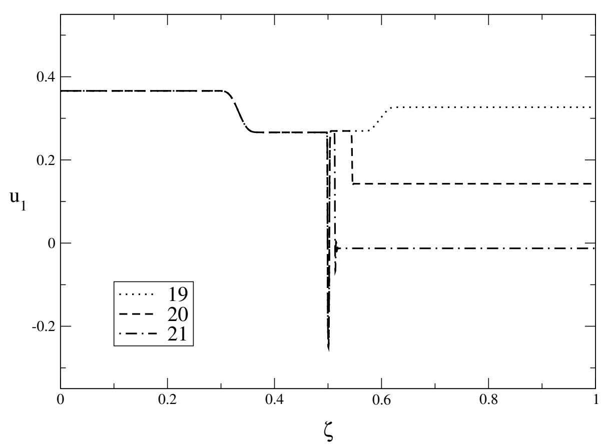

FIGURE 2.25. Riemann solutions 19, 20, and 21: ζ vs. u_1.

[6] E. Doedel and J. Kernévez, *AUTO: Software for continuation problems in ordinary differential equations with applications*, Technical Report, California Institute of Technology, 1986. (Available at http://indy.cs.concordia.ca/auto/doc/index.html.)

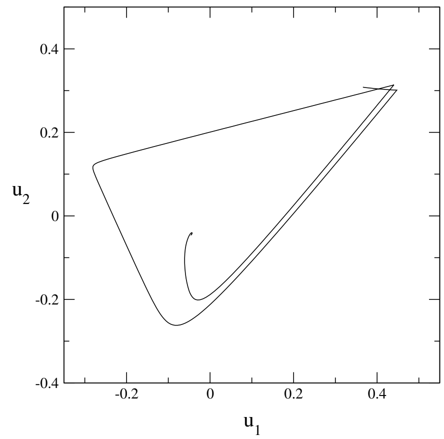

FIGURE 2.26. Riemann solution 23: (u_1, u_2)-plane.

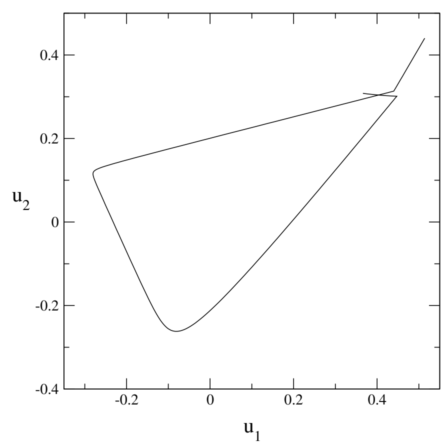

FIGURE 2.27. Riemann solution 24: (u_1, u_2)-plane.

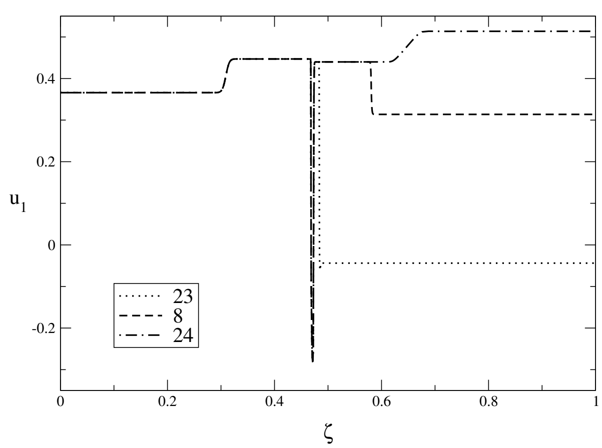

FIGURE 2.28. Riemann solutions 8, 23, and 24: ζ vs. u_1.

[7] N. Fenichel, *Geometric singular perturbation theory for ordinary differential equations*, J. Differential Eqs. **31** (1979), 53–98.
[8] I. Gelfand, *Some problems in the theory of quasi-linear equations*, Uspehi Mat. Nauk. **14** (1959), 87–158; Amer. Math. Soc. Transl. (2) **29** (1963), 295–381.

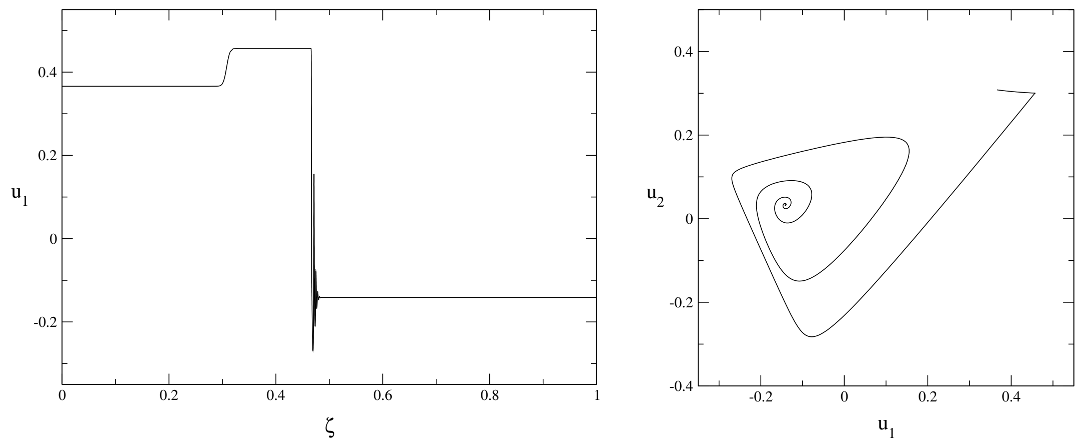

(a) u_1 *vs.* ζ. (b) (u_1, u_2)-plane.

FIGURE 2.29. Riemann solution 22.

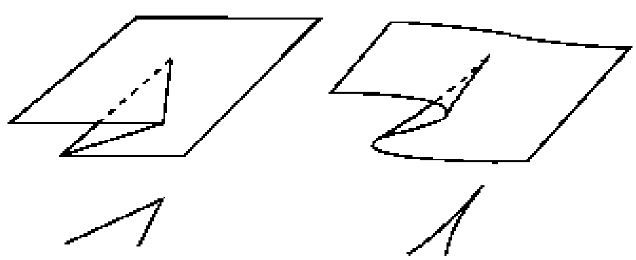

FIGURE 2.30. The space of Riemann solutions and the space of Dafermos-regularized solutions near a cusp point of the latter. Fold curves, as projected onto U_R-space, are shown below the spaces of solutions.

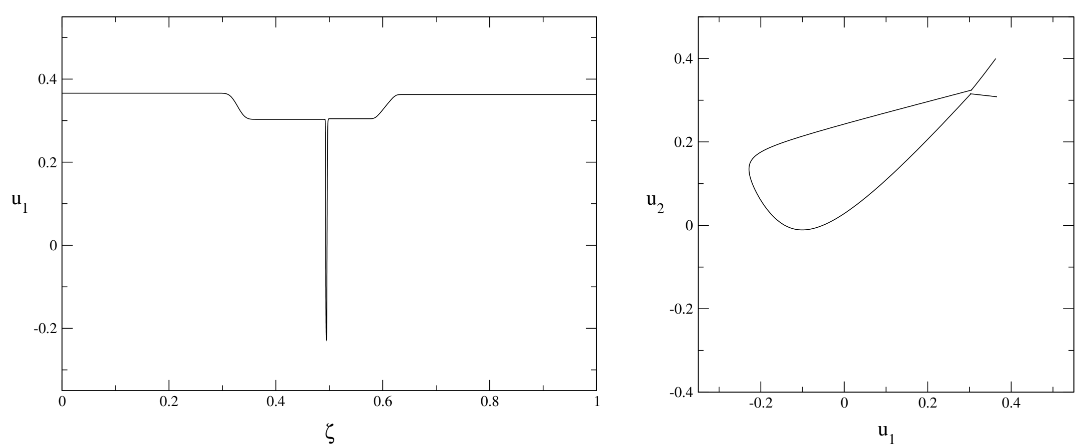

(a) u_1 *vs.* ζ. (b) (u_1, u_2)-plane.

FIGURE 2.31. Riemann solution 25.

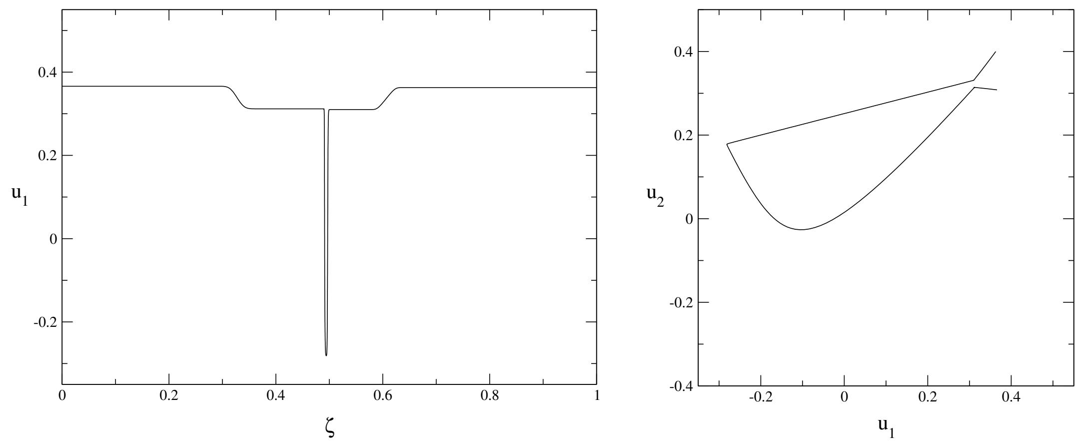

(a) u_1 *vs.* ζ. (b) (u_1, u_2)-plane.

FIGURE 2.32. Riemann solution 26.

[9] J. Goodman, *Nonlinear asymptotic stability of viscous shock profiles for conservation laws*, Arch. Rational Mech. Anal. **95** (1986), 325–344.

[10] C.K.R.T. Jones, Geometric singular perturbation theory. In *Dynamical systems (Montecatini Terme, 1994)*, 44–118, Lecture Notes in Math. **1609**, Springer, Berlin, 1995.

[11] C.K.R.T. Jones and T. Kapper, *A primer on the exchange lemma for fast-slow systems*, in "Multiple Time-Scale Dynamical Systems," C.K.R.T. Jones and A. Khibnik, editors, IMA Volumes in Mathematics and its Applications **122** (2000), 85–132.

[12] T.-P. Liu, *Nonlinear stability of shock waves for viscous conservation laws*, Mem. Amer. Math. Soc. **56** (1985) no. 328, 1–108.

[13] T.-P. Liu, *Pointwise convergence to shock waves for viscous conservation laws*, Comm. Pure Appl. Math. **50** (1997), 1113–1182.

[14] T.-P. Liu and K. Zumbrun, *Nonlinear stability of an undercompressive shock for complex Burgers equation*, Commun. Math. Phys. **168** (1995), 163–186.

[15] T.-P. Liu and K. Zumbrun, *On nonlinear stability of general undercompressive viscous shock waves*, Commun. Math. Phys. **174** (1995), 319–345.

[16] A. Majda and R. Pego, *Stable viscosity matrices for systems of conservation laws*, J. Differential Equations **56** (1985), 229–262.

[17] D. Marchesin, B. J. Plohr, S. Schecter, *Codimension-One Riemann Problems*, J. Dynamics and Differential Equations, **13** (2001), 523–588.

[18] A. Matsumura and K. Nishihara, *On the stability of travelling wave solutions of a one-dimensional model system for compressible viscous gas*, Japan J. Appl. Math. **2** (1985), 17–25.

[19] S. Schecter, D. Marchesin, and B. J. Plohr, *Structurally stable Riemann solutions*, J. Differential Equations **126** (1996), 303–354.

[20] S. Schecter, *Undercompressive shock waves and the Dafermos regularization*, Nonlinearity **15** (2002), 1361–1377.

[21] J. Smoller, "Shock Waves and Reaction-Diffusion Equations," Springer-Verlag, New York, 1983.

[22] P. Szmolyan, in preparation.

[23] A. Szepessy and K. Zumbrun, *Stability of rarefaction waves in viscous media*, Arch. Rational Mech. Anal. **133** (1996), 249–298.

[24] A. E. Tzavaras, *Wave interactions and variation estimates for self-similar zero-viscosity limits in systems of conservation laws*, Arch. Rational Mech. Anal. **135** (1996), 1–60.

[25] K. Zumbrun and P. Howard, *Pointwise semigroup methods and stability of viscous shock waves*, Indiana Univ. Math. J. **47** (1998), 741–871.

Mathematics Department, North Carolina State University, Box 8205 Raleigh, NC 27695
E-mail address: schecter@math.ncsu.edu

Departments of Mathematics and of Applied Mathematics and Statistics, University at Stony Brook, Stony Brook, NY 11794-3651
E-mail address: plohr@ams.sunysb.edu

Instituto de Matemática Pura e Aplicada, Estrada Dona Castorina 110, 22460 Rio de Janeiro, RJ, Brazil
E-mail address: marchesi@impa.br